A methodology to bridge urban shade guidelines with climate metrics

Simon Martinez, Marika Vellei, Manon Rendu, Boris Brangeon, Carlota
Griffon, Emmanuel Bozonnet

A methodology to bridge urban shade guidelines with climate metrics

Simon Martinez [a,b] , Marika Vellei [c,d,e] , Manon Rendu [a,b] , Boris Brangeon [a,b] , Carlota Griffon [f] , Emmanuel Bozonnet [g,b,e,*]

[a] Tipee, 8 Rue Isabelle Autissier, 17140 Lagord, France
[b] RUPEElab, avenue Michel Crépeau, 17042 La Rochelle, France
[c] Univ. Bordeaux, CNRS, Bordeaux INP, I2M, UMR 5295, F-33400, Talence, France
[d] Arts et Metiers Institute of Technology, CNRS, Bordeaux INP, Hesam Universite, I2M, UMR 5295, F-33400, Talence, France
[e] IRSTV FR CNRS 2488 - CENTRALE NANTES 1 Rue de la Noë - BP 92101, 44321 NANTES Cedex 3, France
[f] INSA, 20 Av. des Buttes de Coesmes, 35700 Rennes, France
[g] LaSIE UMR CNRS 7356, Avenue Michel Crépeau, 17042 La Rochelle Cedex 1, France

ARTICLE INFO

ABSTRACT

Urban overheating poses significant challenges to public comfort and health, particularly in pedestrian areas. While urban climate studies offer detailed maps of thermal discomfort and heat stress, urban planning often relies on simplified guidelines, creating a gap between research and practice. This study introduces a methodology to bridge this gap by developing a spatially aggregated dissatisfaction indicator, $PPD*^\wedge$, based on the Universal Thermal Climate Index (*UTCI*) and incorporating a minimum spatial requirement for shade derived from existing cities' shading policies. The novel indicator separately accounts for thermal discomfort in both shaded and sunlit pedestrian areas. A simulated case study in a neighborhood in La Rochelle, France, evaluates six tree planting scenarios, with canopy cover ranging from 0% to 80%. Results indicate that a 20% canopy cover is a practical threshold for mitigating discomfort in moderate and warm climates. This methodology can also be extended to assess additional cooling strategies, such as evaporative systems, and provides valuable insights for optimizing cost-effective and sustainable urban adaptation measures.

1. Introduction

Urban overheating is a major challenge for most of the world's population, which lives in urban areas (United Nations, Department of Economic and Social Affairs, Population Division 2022). The UHI phenomenon is often studied with respect to the health consequences of overheating events on the urban population (Santamouris, 2020, Romero Lankao and Qin, 2011, Wilhelmi and Hayden, 2010, Inostroza et al., 2016, Fard et al., 2021), especially since the 2003 heatwave in Europe. This was particularly noticeable in France, with an excess mortality of up to 40% in small and medium-sized cities, while for larger cities it reached 80% in Lyon and 141% in Paris (Vandentorren et al., 2004).

The increasing occurrence of extreme events highlights the need for cities to propose strategies that mitigate the impact of heat stress and prevent thermal discomfort within inhabited areas (Akbari et al., 2001, Basu, 2009). We propose in this paper a methodology to tackle the issue of overheating in pedestrian zones that considers both how the scientific

community addresses it via heat stress (see section 1.1) and urban climate (section 1.2) models, and the few - much more pragmatic - existing urban policies (section 1.3).

1.1. Heat stress indices at the pedestrian level

To study overheating at the pedestrian level, several types of thermal indices have been developed to express the combined effect of physical (i.e. the four basic parameters of the thermal environment: air temperature, mean radiant temperature, wind speed and humidity), physiological and psychological parameters on human comfort and health and are used to evaluate the thermal quality of urban spaces (Coccolo et al., 2016). The most widely used outdoor thermal indices, such as the Universal Thermal Climate Index (*UTCI*) (Migliari et al., 2022), are all based on thermo-physiological models. Thus, they incorporate both the physical and physiological dimensions of thermal comfort and were all developed based on the concept of an equivalent temperature.

Among these indices, the *UTCI* stands out for two main reasons: 1) it is based on a thermo-physiological model that has been extensively used

---

Nomenclature

PPD [%]   Predicted Percentage of Dissatisfied (*PPD*) people with regard to their thermal comfort

PPD* [%]   *PPD* in the sunny areas of the neighborhood pedestrian zones

PPD** [%]   *PPD* in the sunny areas minus the people moving to the pedestrian shaded areas

PPDˆ [%]   *PPD* in the shaded areas of the neighborhood pedestrian zones

PPD*ˆ [%]   *PPD* in the whole neighborhood pedestrian zones

σ ˆ [%]   Percentage of the area of the neighborhood pedestrian zones that is shaded

σ ˆ$_{forAll}$ [%]   Minimum shade ratio to ensure that all pedestrians are provided with shade

UTCI [°C]   Universal Thermal Climate Index

UTCI* [°C]   *UTCI* in the sunny areas of the neighborhood pedestrian zones

UTCIˆ [°C]   *UTCI* in the shaded areas of the neighborhood pedestrian zones

and validated (Psikuta et al., 2012, Katić et al., 2016), and 2) it is easier to apply as it does not require input on the clothing and activity level of the person. Indeed, the *UTCI* incorporates an adaptive clothing model (Havenith et al., 2012) and fixes a representative outdoor activity to a walking speed of 4 km/h (2.3 met), which is adequate for assessing pedestrian thermal discomfort and stress.

To further assess the thermal sensation of a group of individuals, one can use the traditional *PPD* approach (Predicted Percentage of Dissatisfied) defined by Fanger (2017 ASHRAE Handbook: Fundamentals 2017). This standardized approach is particularly interesting for our study, since we are considering a large pedestrian area with different individual profiles. Then, based on existing studies that correlate *UTCI* and *PPD*, we present in more detail this approach, which includes the calculation of a new *PPD*ˆ* indicator in section 3.

1.2. Urban climate analysis at the neighborhood level

Unlike weather stations at a few specific urban locations, detailed numerical modeling provides access to a rich vein of information on the spatial and temporal variations of the urban climate variables (Bozonnet et al., 2015). This detailed numerical climate information can be combined with heat stress indices to provide thermal discomfort and stress maps. Middel et al. (Middel et al., 2017) have demonstrated the value of this approach by predicting the coolest pedestrian routes during extreme heat events in Phoenix. Their study optimized pedestrian exposure by determining the route with the minimum average heat stress. The perspectives of such detailed heat stress maps are multiple, from providing real-time route guidance to providing urban planners with a tool to quantify the real impact of future strategies.

However, many urban climate studies ignore the proper use of thermal comfort results, mapping and averaging pedestrian thermal discomfort indices, such as the *UTCI*, without any consideration for the actual use of the public space, by including boulevards or pitched roofs. These acceptable simplifications in the process of numerical development papers that focus on the capabilities of the models, e.g. (Ding et al., 2024), become critical in papers which use commercially available tools and claim to provide expertise and advice to urban planners.

The work by Huang et al. (Huang et al., 2022) is an example of a better way of using thermal discomfort indices. The authors both recorded and simulated thermal conditions in Hong Kong neighborhoods to correlate *UTCI* mapping results with the residents' use of outdoor spaces. Older people were more likely to use outdoor spaces, but their presence was also more sensitive to high *UTCI* events. Although the simulation tools provided an overview of the spatial variation of *UTCI* and shading areas, only one *UTCI* temperature per time step was ultimately used in their analysis. This is common in urban simulations, where spatial variation is shown for a few moments, while temporal variation is studied with simplified spatial temperature averages or extremes.

Many examples in the urban climate literature illustrate the diversity in the use of detailed climate maps to quantify the benefits of planning strategies (Aleksandrowicz and Pearlmutter, 2023, Rüdisser et al., 2021, Barone et al., 2024, Buo et al., 2023). This demonstrates (1) the importance of spatial and temporal details of climatic variability, (2) the unmet challenge of developing methods to translate the sparse information available into useful summary indicators (e.g oversimplifications of averaged values), and (3) the limitation of detailed maps for non-experts, which maintains the disconnect between urban planning and climate modeling.

As a result, planners often focus on practical strategies, especially by defining shading policies since mean radiant temperature is known to be the main factor influencing heat stress.

1.3. An empirical approach to urban overheating through shading policies

In contrast to the highly detailed scientific approaches, urban planning policies often address urban overheating with much more practical and qualitative objectives. Urban heat adaptation plans are mainly aimed at raising awareness in vulnerable populations (Sampson et al., 2013) and limited to understanding the overall mechanisms. They are usually presented as guides, e.g. the Red Cross Red Crescent Climate Centre Heatwave Guide for Cities (Singh et al., 2019), promoting common or locally accepted mitigation strategies.

In practice, the level of involvement of cities varies widely, as highlighted by a recent study by Ulpiani et al. (Ulpiani et al., 2024) which reviewed over 2500 European urban policies on how they account for urban overheating. This policy review showed that while the most exposed cities are acting against urban overheating, historically temperate areas remain less concerned despite growing climate risks. Several cities are more actively involved in voluntary action plans for a much higher level of requirements and short-term results, such as the European Initiative of Climate-Neutral Cities by 2030 (NetZeroCities, 2024) or the Phoenix Adaptation Plan (City of Phoenix 2010), which specifically includes a target of 25 % tree canopy cover by 2030 to combat urban overheating. While typical urban policies (Ulpiani et al., 2024, Dhalluin and Bozonnet, 2015) refer to blue and green or nature-based solutions, such as tree shading and evaporative cooling from water ponds, fountains and vegetation, and grey solutions, such as increasing urban albedo, more and more urban planning regulations emphasize the proximity of parks, the concept of cool pathways, and the necessary creation of shade, either through trees or artificial structures (Turner et al., 2023). We focus here on the urban shade strategy, which is not new as it can be observed in vernacular cities, especially in hot and arid climates that have narrow streets and traditionally incorporate shade (Peeters et al., 2020). However, this is a common problem in modern cities, and especially in poor urban settlements which would require more consideration of urban shading, as highlighted by Turner et al. (Turner et al., 2023).

In this context, we have reviewed and identified in Table 1 a collection of urban policies that provide an overview of how some cities worldwide are working toward specific shading goals.

The variety of values indicates a first attempt to provide quantitative targets or "performance" results. All cities outlined in Table 1 are particularly concerned with both the livability of their outdoor spaces and their exposure to extreme heat. In some cities, such as Dubai and Phoenix, pedestrian shading is even enforced by local building codes (Government of Dubai, 2021, City of Phoenix 2024). The magnitude of the recommended ratio of tree canopy cover, or shading of pedestrian

Table 1
Quantitative targets from some urban policies related to urban shading of pedestrian areas to reduce urban overheating

Location	ASHRAE climate zone	Recommendation	Shade calculation	Mandatory	Ref
Singapore	0A Extremely hot humid	*Open-spaces shading* Privately owned public spaces Minimum 50%	June 21 at 9am, 12pm and 4pm	YES	(Urban Redevelopment Authority (Singapore) 2023)
Dubai	0B Extremely hot dry	*Open-spaces shading* School playgrounds Minimum 30%	No reference	YES	(Government of Dubai, 2021)
		Open-spaces shading Building surroundings Minimum 50% (trees, solar panels, or other structures), or other UHI strategies	No reference	YES	
		Continuous shaded paths Minimum 50 m intervals (public spaces)	Not relevant	YES	
Phoenix, US	1B Very hot dry	*Building sidewalk shading* Minimum 75% Including trees, buildings and other structural shades	June 21 at 12pm	YES	(City of Phoenix 2024)
		Open-space shading Minimum 50% of which 50% minimum from trees		YES	
		Cool corridors program Minimum 30% shading 0.4 to 0.8 km shaded sidewalks 60% shading is rated excellent	During the hottest times of the day	NO	(City of Phoenix 2022)
		Tree canopy cover (city) Minimum 25% by 2030	Non-relevant	YES	(City of Phoenix 2010)
Tel-Aviv, Israel	2A Hot humid	*Tree canopy cover (streets)* 50-60% in old streets When street infrastructure does not permit a minimum shading, canopy area cover of 60%	Not relevant	NO	(Peeters et al., 2020)
Melbourne, Australia	3A Warm humid	*Tree canopy cover* from 22% (present) to 40% by 2040	Not relevant	YES	(Urban Forest Strategy 2014)
Grenoble, France	4A Mixed humid	*Sidewalk and open-space shading* Minimum 40%	June 21 at 2pm	NO	(Bertrand et al., 2014)

areas, varies from 40% up to 75% around buildings in Phoenix (USA), which is also the city that is most committed to mandatory targets. The Phoenix Adaptation Plan (City of Phoenix 2010) specifically includes a target of 25 % tree canopy cover by 2030 to address urban overheating.

However, there is no real correlation between these targets and the real heat stress that can be computed from detailed models: quantifying heat stress to conduct cost-benefit analyses of overheating mitigation plans is still a challenge for policymakers.

2. Research gaps and novelty

As highlighted in the previous policy review, despite the lack of practical tools and indicators, there is a growing number of voluntary initiatives to quantify the effectiveness of urban adaptation strategies to define concrete urban planning goals. Both the traditional shading architecture of hot cities, and new climate change adaptation plans, can benefit from better knowledge of the detailed distribution of heat stress within neighborhoods.

In the following sections, we aim to propose a methodology that can address the following two research gaps:

1. **Pedestrian thermal discomfort and stress needs to be quantitatively and spatially adequately (by separating between shaded and sunlit areas) accounted for in optimal shading ratio calculations.** Some authors have proposed the calculation of the optimal tree canopy cover ratio, such as Peeters et al. (Peeters et al., 2020) or Li et al. (Li et al., 2023). Another study by Aleksandrowicz et al. (Aleksandrowicz et al., 2020) on urban shading and heat stress in Tel Aviv (Israel) derived the Shading Index *SI*. However, these studies did not quantitatively correlate shading ratios with pedestrian thermal discomfort and stress, aside from qualitative analyses of detailed maps.
2. **A minimal spatial requirement for shade needs to be included in optimal shading ratio calculations.** What is the point of having a comfortable shaded place if the area is too small? A minimum cool place availability should be accounted for.

We propose a new methodology to derive an indicator that can be used to address these gaps and demonstrate its use in a new neighborhood in La Rochelle, France that represents our case study. This indicator is defined at the neighborhood level and accounts for the shaded surface ratio (Fig. 1b) and thermal discomfort both in shaded and unshaded areas (Fig. 1c). The local climate of the case study is simulated using well-known microclimate models. This provided the climate data needed to create *UTCI* maps for the neighborhood. (Fig. 1a). However, the overall methodology does not depend on the specific microclimate or physiological models chosen, and it is important to note that in this study we do not discuss the validity of these commonly used models.

3. Methodology

3.1. Overview

The proposed methodology (Fig. 1 and Table 2) relies on the usual tools for urban climate and outdoor thermal comfort index calculations (Table 2b), together with further analysis of shade availability (Table 2a), to compute the new pedestrian overheating index (Table 2c).

This procedure, detailed below, is processed in three main stages:

- Having access to detailed data of the modelled neighborhood, including building geometry and usage, land use, and pedestrian areas, defined by the urban planners (Table 2a). This data is typically processed in GIS software; the source database and availability can differ from one city to another, and we illustrate typical sources with our case study presented in section 4;
- Carry out typical urban microclimate simulations (Table 2b) which require GIS data as input; we used well-known software (see 3.2) for the thermal environment characterization, which is required for thermal comfort calculation (see 3.3);
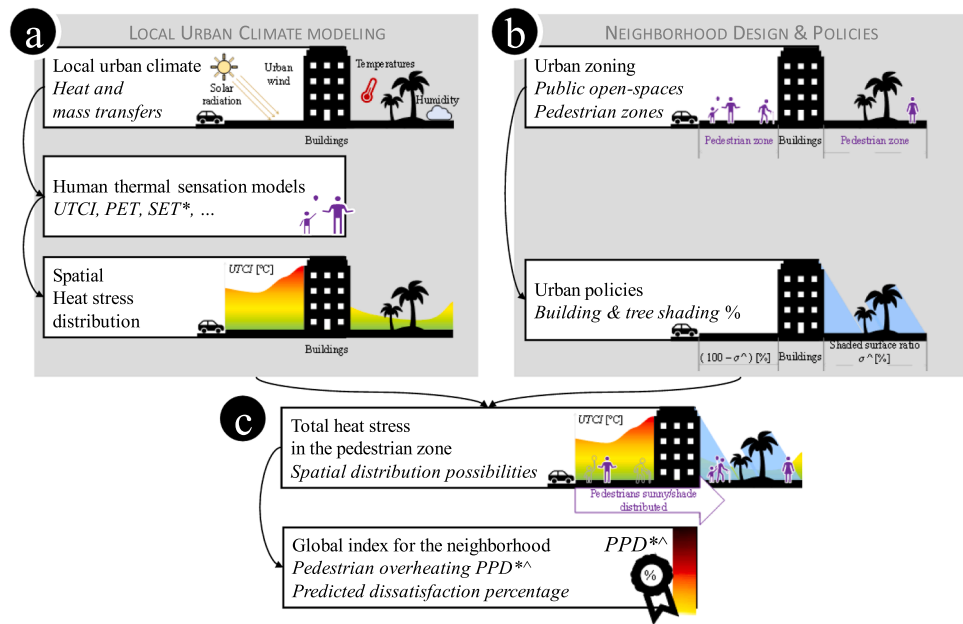
Fig. 1. Illustration of our approach to bridge the gap between (a) detailed local urban climate modeling, and (b) urban practice and design rules, in order to (c) define a quantitative rating process for climate adaptation strategies.

Table 2
Overview of the numerical simulation tools used in this study

Purpose	Inputs	Numerical tools	Outputs
(a) Neighborhood design and data management	3D geometry Pedestrian zone locations Tree planting and shading structure implementation	GIS platform (*QGIS*) Online databases (BDtopo, OSM, etc.)	Urban morphology and design indicators (Tree cover ratio, Building density, etc.)
(b) Urban climate	Urban radiative properties 3D numerical mockup	Thermoradiative model *Solweig* (Lindberg et al., 2008)	Mean radiant temperature [°C] maps
	Rural weather data Urban morphology indices Building data	Urban canopy air temperature *UWG* (urban canyon model) (Bueno et al., 2012)	Urban air temperature [°C]
	Meteorological wind Tree and building sheltering distribution	Urban wind model *URock* (Bernard et al., 2023)	Wind velocity [m/s] maps
	All previous urban climate outputs	Physiological equivalent temperature model *PyThermalComfort* (Tartarini and Schiavon, 2020)	*UTCI* equivalent temperature [°C] maps
(c) Neighborhood heat stress rating	*UTCI* maps Pedestrian zones	Specific Python code	*PPD* *^

- Then, the core of our methodology was to define an overheating indicator (Table 2c) that includes both urban planning data and thermal discomfort distribution, which is quantified by a dissatisfaction index *PPD**^ (as defined in section 3.5).

The Python code used to process and prepare the simulation input data is openly available via our repository (https://github.com/rupeela b17/pymdu).

3.2. Urban microclimate simulations

We present here the simulation tools (thermoradiative, urban canopy temperature, and urban wind) used to determine the thermophysical variables necessary for the characterization of the local urban climate conditions (Table 2b).

The Solweig software (Lindberg et al., 2008), which has been used in many urban research studies (Ding et al., 2024, Buo et al., 2023, Aleksandrowicz et al., 2020), provides a detailed distribution of pedestrian-scale mean radiant temperature within a neighborhood. Solweig simulates shading phenomena by taking into account the shading effect of buildings and other urban structures. We developed a database management software (Table 2a) to collect and preprocess geographical and urban data to define the urban area's geometry, including building height and shape, local topography, and vegetation. For building shaded areas, the model calculates a reduced incident solar irradiance, while for trees a 3% light transmittance is assigned by default. The surface temperature model makes some simplifications that speed up the calculation over the full season of the detailed neighborhood maps required for our study objectives. The surface temperature correlations used by Solweig are based on experimental data specific to urban environments and other environmental variables such as solar radiation, surface emissivity, air temperature, and wind speed.

The air temperature in the urban canopy is then given by the Urban Weather Generator (UWG) code (Bueno et al., 2012), which is widely described and used in the scientific community (Nakano et al., 2015, Bueno et al., 2013, Martinez et al., 2021). In this model, the relationship between the reference weather station and the mesoscale urban boundary layer is taken into account to calculate the urban canopy layer temperature, which is often modelled in the literature using the mesoscale model WRF (Ding et al., 2024). The UWG model includes sub-models that quantify heat exchanges at the reference station, known as the rural station, typically located in suburban areas near an airport. It also incorporates a vertical heat diffusion model for the rural site, an urban boundary layer model to estimate heat exchanges above the urban canopy, and a street canyon model to determine microclimatic parameters within the city. Relative air humidity is then calculated, taking into

account the change in air temperature and the humidity ratio given by the reference weather data. This assumption, which could be further explored with more detailed models, is typically used for evaporative cooling strategies such as urban lawns, which mainly affect the local surface temperatures.

Finally, the detailed urban wind airflow is provided by URock (Bernard et al., 2023), an open-source Python implementation of the Röckle model (Rockle, 1990) used in various urban studies and previously implemented in the QUIC-URB software (Bestimmung der Strömungsverhältnisse im Bereich komplexer Bebauungsstrukturen 1990, Singh et al., 2008). Unlike detailed CFD tools, which require detailed meshes and therefore long computation times, this model allows a fast calculation of wind velocities throughout the season by determining wind topology, and the zones of influence of urban obstacles, as an empirical function of their geometry, given the reference wind directions and intensities. We then extract the perceived wind at pedestrian level from the fully detailed 3D calculation, which is extrapolated at $z = 10$ m with the standard wind profile in order to meet the assumptions of the *UTCI* formula.

3.3. From the UTCI to the percentage of dissatisfied PPD

The previous set of urban thermophysical outputs is used to calculate the *UTCI* equivalent temperatures (Bröde et al., 2012) over the whole neighborhood (see Fig. 1a) using the open-source Python package PyThermalComfort (Tartarini and Schiavon, 2020). We then applied the linear relationship proposed in Bröde's study (Bröde et al., 2012) to convert the *UTCI* into a thermal sensation vote on the classic 7-point ASHRAE scale, ranging from -3 ("cold") to +3 ("hot"). Next, to map the thermal sensation to a percentage of dissatisfaction, we used Fanger's sigmoid relationship, which links the Predicted Percentage of Dissatisfied (*PPD*) to the Predicted Mean Vote (*PMV*), as shown in equation (1) (2017 ASHRAE Handbook: Fundamentals 2017). The resulting equation (2) directly relates *PPD* to *UTCI* as illustrated in Fig. 2.

$$PPD = 100 - 95 \cdot \exp\left(-0.03359 \cdot PMV^4 - 0.2179 \cdot PMV^2\right) \quad (1)$$

$$PPD = 100 - 95\exp$$
$$\left[-0.03359\left(2.5\frac{UTCI - 26°C}{38°C - 26°C} + 0.5\right)^4 - 0.2179\left(2.5\frac{UTCI - 26°C}{38°C - 26°C} + 0.5\right)^2\right] \quad (2)$$

To study the effect of pedestrian heat stress, we only focused on the warm and hot side of the *PPD* curve by varying the *UTCI* between 26 and
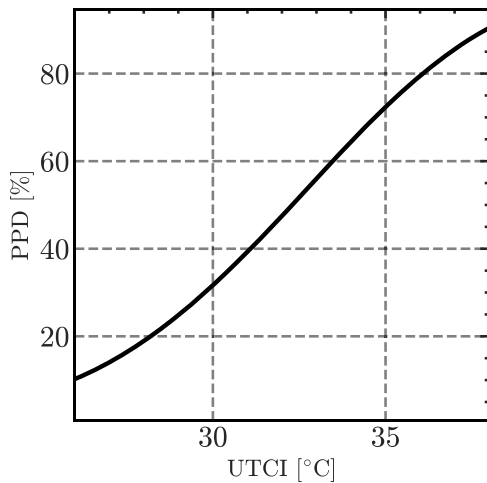

Fig. 2. Relationship between *UTCI* [°C] and *PPD* [%] obtained from the Bröde study (Bröde et al., 2012) and *PPD* analytical expression (2017 ASHRAE Handbook: Fundamentals 2017).

38°C, as defined in equation (2). Thus, we did not consider the cold dissatisfied outdoor occupants as in the study of Hwang et al. (Hwang et al., 2022). For an analysis of cold events, our approach would require further investigation, particularly regarding cold wind corridors.

From the spatially distributed *PPD* values, we calculated two distinct summary spatial metrics: the spatially averaged *PPD* in shaded areas (*PPD^*) and the spatially averaged *PPD* in sunlit areas (*PPD**) at each time step. These values indicate the percentage of dissatisfaction in both areas, with ^ and * denoting shaded and sunlit values, respectively (Fig. 3).

We also calculated the average equivalent temperature in the shaded and sunlit areas of the pedestrian zones in the neighborhood, represented as *UTCI^* and *UTCI**, in degrees Celsius. As observed (see section 1.21), the *UTCI* equivalent temperature is strongly influenced by shading and the mean radiant temperature during overheating events. This portioning between shaded and sunny areas (given by the percentage $\sigma^$ and $(1 - \sigma^)$ in Fig. 3) is therefore consistent with many previous studies that primarily considered the sky view factors or the mean radiant temperature as factors affecting urban heat discomfort. In a future study, this approach could be improved further by considering the dynamic behavior of pedestrians, which is a limitation of the standard thermal sensation indices that are defined for a stationary state.

3.4. A shading ratio policy threshold

To correlate the thermal dissatisfaction (*PPD^* and *PPD**) with the availability of cool shaded areas, we need a definition of the area required to shade 100% of pedestrians. This would depend on many factors, such as the level of crowding acceptable to the local population, the number of people, which may vary throughout the day, the acceptable discontinuity of shaded areas or the maximum acceptable distance to a shaded area. In addition to these uncertainties, there are many other constraints, both economic and structural, that limit the availability of shaded areas. However, the strict optimum that was given by previous studies does not adequately consider the overheating stress, as underlined in the first section (see 1.3).

Therefore, we will set in the following a "forAll" shade ratio that can be reasonably achieved, ensuring that 100% of pedestrians in the neighborhood are able to shade themselves, that shaded areas are close enough to walk to, and that there is enough space for everyone. This input parameter cannot be considered as the ideal result of the following calculations that takes thermal sensation into account.

From the review of urban shading policies (see Table 1 in section 1.3), we found that in cities where overheating stress and the value of shade are quantitatively addressed, the shading ratio objectives varies between 40% to 70%, also depending on their climate zone, as cooler seasons also require sufficient sunny areas. We adopt in the following the lower value $\sigma^_{forAll} = 40\%$. This value takes into account not only tree shade, but also artificial structures and buildings, and was determined in consultation with experts for our case study. The effective surface shading ratio $\sigma^$ [%] is calculated at each time step from the solar radiation simulations and is compared to the "forAll" ratio $\sigma^_{forAll}$ [%], while $\sigma^* = (1 - \sigma^)$ [%] is the sunny fraction. In the following section, this shading ratio threshold $\sigma^_{forAll}$ is then used to define a
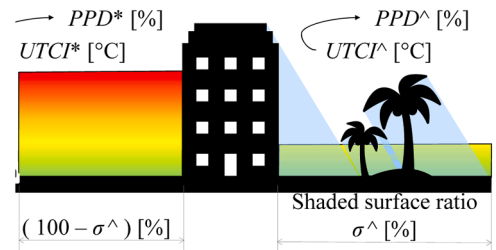

Fig. 3. Shaded and sunlit definitions of heat discomfort indices.

global *PPD* that considers both the heat stress and the spatial distribution of pedestrians.

3.5. Global PPD definition based on shading ratio and thermal map

We will first illustrate with a simplified example our methodology for predicting a global percentage of dissatisfied *PPD*^* related to both heat stress and shading in the whole neighborhood, for which we will then define the calculation formulae. For this explanation, we considered the following simplified climatic situation where the difference between shaded and sunlit areas is only due to the mean radiant temperature (Fig. 4), which was obtained using the microclimate simulation tools (section 3.2).

Given a representative sample of 100 pedestrians, the previous equation (2) allowed us to predict both dissatisfaction percentages for sunlit and shaded zones (*PPD** and *PPD^*), which we analyzed by considering the 100 pedestrians in the sunlit zone in an initial state (Fig. 5a).

A *PPD** = 70% in the sunlit zone given in the example means that 70 dissatisfied pedestrians would spontaneously seek refuge in the shade (Fig. 5a right). The lack of shaded area is given here by the shade availability ratio ($\widehat{\sigma}$ / $\widehat{\sigma}_{forAll}$), which is defined by the effective shading ratio $\widehat{\sigma}$ at this time of the day (Fig. 4), and the shading ratio $\widehat{\sigma}_{forAll}$ defined in Section 3.4.

In the "high shading ratio scenario" (Fig. 5b), the available shade is sufficient for all dissatisfied pedestrians in the sunlit area given that the effective shading ratio $\widehat{\sigma}$ is higher than $\widehat{\sigma}_{forAll}$ ($\widehat{\sigma}$ / $\widehat{\sigma}_{forAll}$ = 120%). However, there are still 40 dissatisfied people in the shade out of a total of 100 pedestrians in the neighborhood, since the number of thermally dissatisfied pedestrians in the shade is 40% (Fig. 5a right). Then, for this example, the global *PPD*^* is the same as the shaded zone *PPD^*, i.e. 40%.

In the "average shading ratio scenario" (Fig. 5c), the shading ratio is enough only for 50 people ($\widehat{\sigma}$ / $\widehat{\sigma}_{forAll}$ = 50%). Compared to the 70 people (70% = *PPD**) who seek shade, 20 are dissatisfied as they are now in the sunlit zone. Out of 50 people in the shade, there are still 30 people who feel comfortable, and 20 dissatisfied, resulting in a total dissatisfied ratio of 40.

Then, for all these scenarios, the ratio of pedestrians able to move to the shade is given by the more general equation (3):

$$\min\left(PPD^*, \frac{\widehat{\sigma}}{\widehat{\sigma}_{forAll}} \right) \tag{3}$$

We note *PPD*** the percentage of dissatisfied people who stay in the sunlight (Fig. 5c). This value can be expressed by equation (4) as the difference between *PPD** and the previous group who move effectively to the shade.

$$PPD^{**} = PPD^* - \min\left(\frac{\widehat{\sigma}}{\widehat{\sigma}_{forAll}}, PPD^* \right) \tag{4}$$

In the "low shading ratio scenario" (Fig. 5d) the shading ratio is enough only for 20 people ($\widehat{\sigma}$ / $\widehat{\sigma}_{forAll}$ = 20%). Compared to the 70 people (70% = *PPD**) who seek shade, only 20 people can feel

comfortable in the shade, which makes a total of 50, including the 30 people who felt comfortable in the sunlit zone. So, there is a total of 50 dissatisfied people, i.e. *PPD*^* = 50%.

Finally, the general formula to evaluate the dissatisfaction percentage of the whole neighborhood can be expressed in equation (5), which is consistent with the three previous scenarios.

$$\widehat{PPD}^* = PPD^{**} + \min\left(\max(0, \ \widehat{PPD} - PPD^{**}), \frac{\widehat{\sigma}}{\widehat{\sigma}_{forAll}} \right) \tag{5}$$

This *PPD*^* formula is consistent between both limits: the "lower limit" *PPD*^* = *PPD^* when there is 100% shade or that there is shade for everyone ($\widehat{\sigma} \geq \widehat{\sigma}_{forAll}$), and the "upper limit" *PPD*^* = *PPD** when there is no shade available ($\widehat{\sigma} = 0$). All of the above reasoning is valid given that people seek shade; otherwise, if *PPD^* > *PPD**, a similar expression could be proposed by replacing *PPD** by *PPD^* and vice versa, and $\widehat{\sigma}$ by $(1 - \widehat{\sigma})$, which could constitute a future study for cold season conditions.

4. Case study

4.1. Location and hypotheses

The selected oceanic climate case study (ASHRAE climatic zone 4A, mixed-humid), the Atlantech neighborhood in the suburb of La Rochelle, France (latitude 46.1847, longitude -1.14670), is a redeveloped neighborhood consisting of 1375 buildings (Fig. 6).

The selected area of interest is approximately a square of 1 km × 1 km, and we developed the scripts to automatically process the input data from geographic databases, the urban planning strategy for the pedestrian zone that we define in the GIS, and weather data. In order to automate the preprocessing of different urban planning strategies, which could be replicated in any other neighborhood, we made the following assumptions:

- Buildings were automatically located and processed, while for land cover other than buildings we included a limited number of surface typologies, such as asphalt, vegetation, water, and bare soil (Fig. 6);
- The pedestrian zone, which includes both large open spaces and sidewalks along streets, was manually delineated (hatch marks Fig. 6);
- The shading strategy of the neighborhood was defined by the addition of the tree canopy, while the buildings and their shading effects were not modified. We automatically distributed trees in the pedestrian zone, represented as vertical cylinders of 4 m in diameter and 6 m high (see the tree planting layout in Fig. 6). The solar transmittance of the tree canopy is highly dependent on the tree species. We assumed the foliage had a total solar transmittance of 3%, which is in the range of the observations made by Konarska et al. (Konarska et al., 2014), who found 1.3 to 5.3% for urban foliated tree crowns of common species from Northern Europe.

4.2. Weather data

The Weather data are given by the typical meteorology (TMY) of the case study location, La Rochelle, France. However, in order to further study the impacts of extreme overheating on our methodology, we also examined the theoretical weather (Fig. 7) of Phoenix (USA), which is classified as a very hot dry climate (ASHRAE climate zone 1B). Located in the middle of the desert, Phoenix is pushing shading policies and concerned about urban overheating, making it an interesting case to assess the robustness of our method.

For the simulation period from June 1 to August 31, we could clearly identify the differences in climate conditions in the average daily air temperature shown in Fig. 7, since the minimum daily variations in Phoenix are above the average temperatures of La Rochelle. Additionally, the annual evolution of air temperature, humidity, wind speed, and
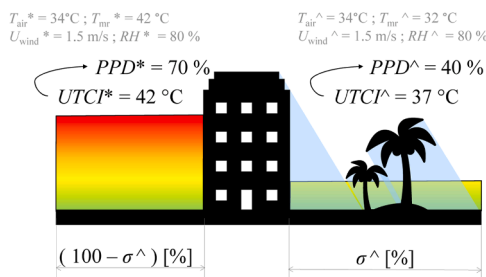
Fig. 4. Theoretical thermal sensation results in shaded (^) and sunny (*) zones to illustrate the methodology
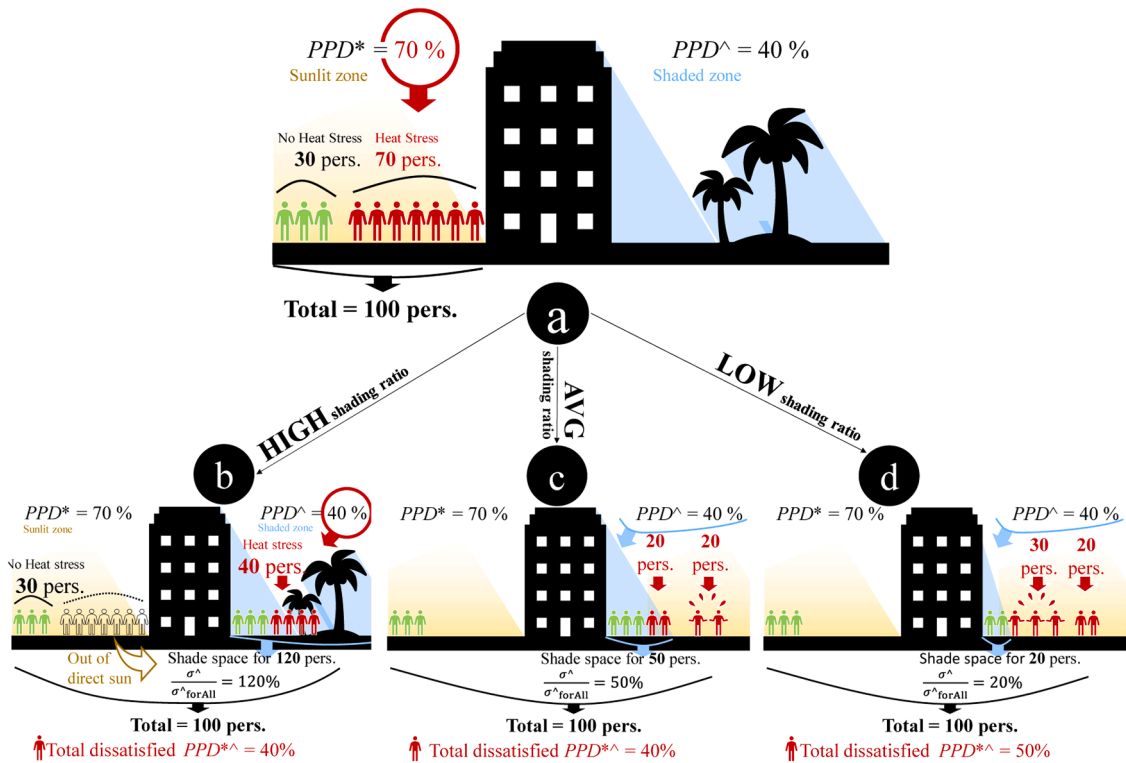
Fig. 5. Example of a 100 pedestrian sample – (a) Initial pedestrian heat stress under sunlit areas, and (b,c,d) the cumulated heat dissatisfied percentage (*PPD**^) for both sunlit and shaded zones at three different shade capacities.
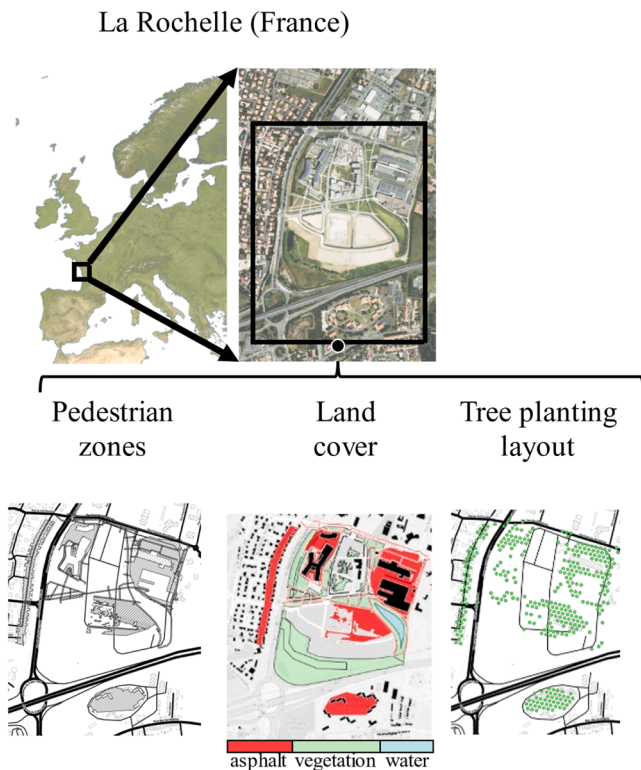

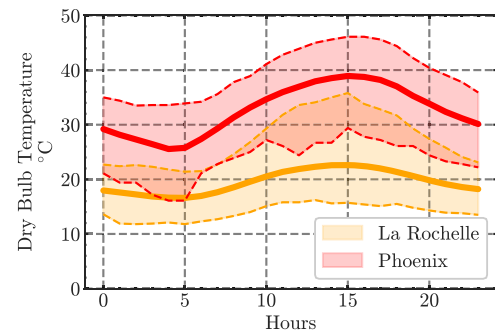**Fig. 6.** Case study location, aerial photo, pedestrian land cover and tree planting strategy.

Fig. 7. Average and extreme daily dry bulb temperature for La Rochelle (yellow) and Phoenix (red), for the period from June 1 to August 31.

the wind rose are plotted and presented in the appendix.

4.3. Tree planting strategies

Given the very sparse distribution of trees, the current tree cover is low, ranging from 0 to 5%, which is typical for the La Rochelle area and which will likely be improved by urban plans and future tree planting objectives.

Then, in the following study, we varied the tree canopy cover of the pedestrian zone from the no-tree base case scenario up to approximately 80%, given the theoretical and regular tree layout generated for a standard comparison as represented Fig. 8. The black-bordered labels are included to guide the reader, with the exact percentage indicated below each label.

We checked that the calculated effective shading surface ratio $\sigma^{\hat{}}$ obtained with Solweig for the summer solstice at 2 pm was relatively close to the theoretical surface ratio of the tree canopy to the pedestrian surface for the 6 scenarios (Fig. 8).
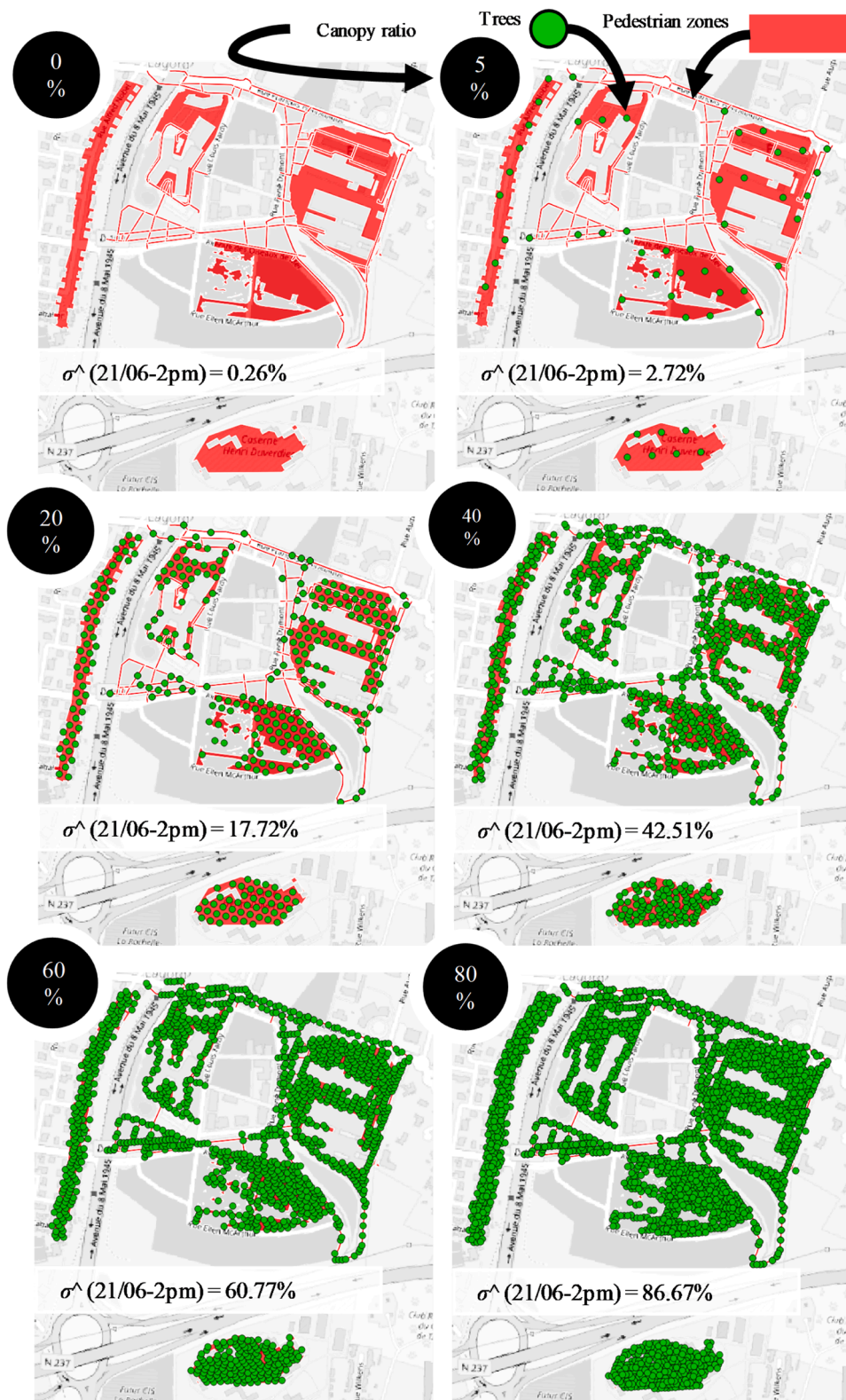
Fig. 8. Various tree layouts and canopy covers (0, 5, 20, 40, 60 and 80%) for the parametric study.

5. Results and Discussion

First, we will present the results of the microclimate simulation necessary for the further calculation of the previously defined $PPD*\hat{}$ indicator, which is discussed in relation to the parametric variation of the tree canopy and climate warming. Although the numerical models are spatially detailed for the large volume of the case study, their efficiency allowed us to compute all the detailed climate maps for the entire summer period from June 1 to August 31, and an hourly time step.
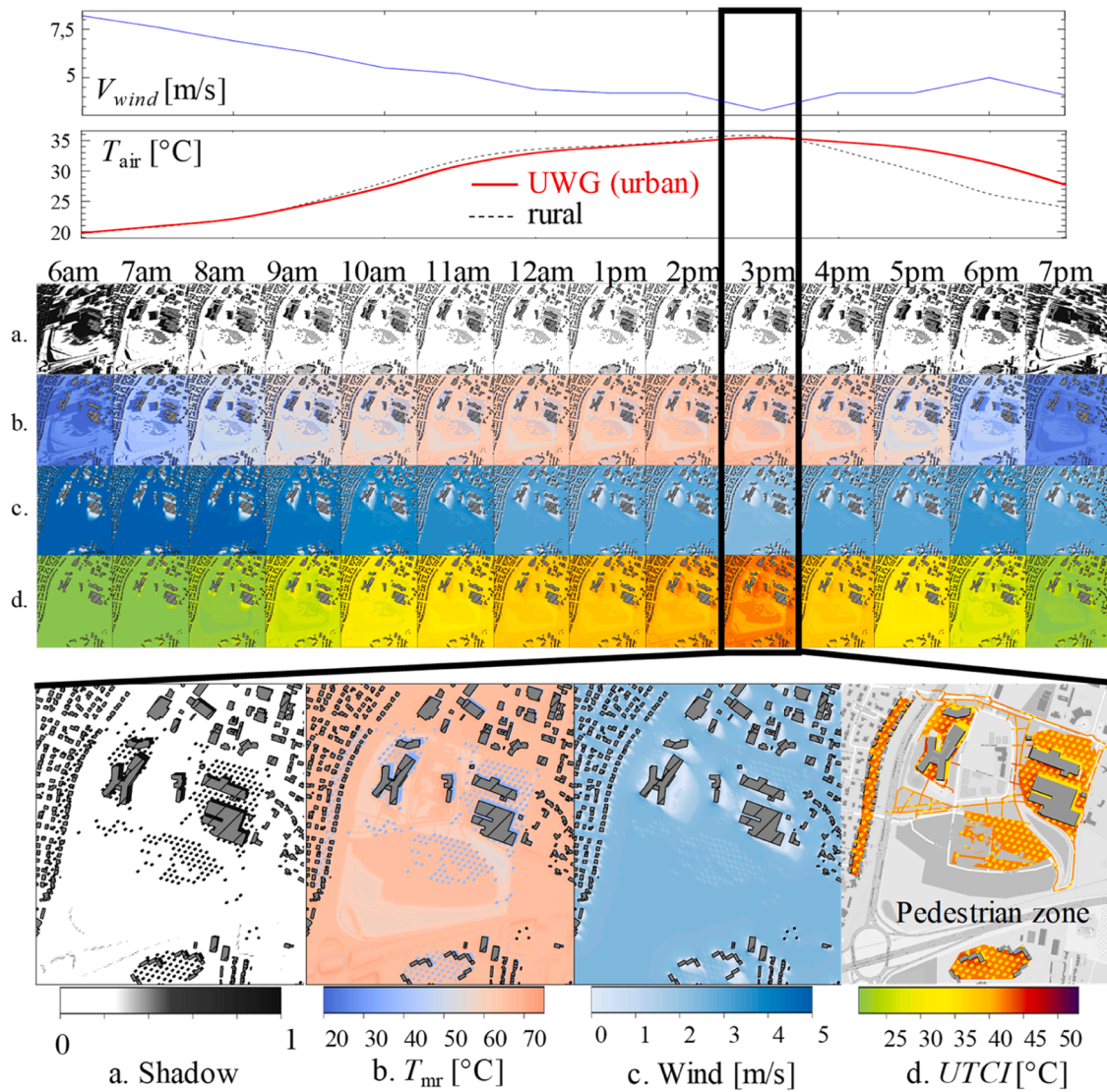
Fig. 9. Detailed pedestrian level results – (a) shading, (b) mean radiant temperature (from SOLWEIG), (c) wind speed (from U-Rock) and (d) *UTCI* (from pythermalcomfort)– August 11, from 6am to 7pm.

5.1. Urban microclimate

To visualize the typical detailed simulation results with a 1m × 1m mesh resolution, we first present the diurnal climate maps (Fig. 9), including shading, mean radiant temperature, wind speed, and *UTCI* at the pedestrian level for the hottest day of the three-month period (August 11) for the reference case study using La Rochelle TMY data and 20% canopy cover. We specifically extracted the equivalent temperature in the pedestrian area (Fig. 8).

This typical summer day is particularly hot for pedestrians at 3 pm in terms of the equivalent temperature *UTCI* [°C]. The change in shading during the day (first row in Fig. 9) obviously had an impact, although this indicator alone is obviously not totally correlated to the heat stress characterized by the *UTCI*, underlining the limitations of simplified approaches based only on the sky view factors or the shading ratios. In more detailed analyses, the mean radiant temperature (second row in Fig. 9) is often used to assess urban heat stress. Although it correlates better with the *UTCI* than shading maps, we observed a clear difference between the hottest time at 3 pm and earlier time steps with similar mean radiant temperatures, which can be explained here by the significantly reduced wind speed (third row in Fig. 9) at this time of the day. This parameter is important because tree canopies reduce wind speed, counteracting some of the shading benefits. This effect is visible on the maps, especially in the leeward zones of buildings. This result underlines the importance of a full analysis of the thermal sensation, which can be approximated by a physiological model such as the equivalent temperature *UTCI*. A closer look at these maps shows typical effects, like shading significantly reducing mean radiant temperature, or the small impact of sun-exposed water surfaces, which could inform urban planning and expert analysis for specific scenarios. However, there are too many more climate maps to analyze (taking into account other urban design strategies and other seasons) which are much more complex to differentiate without a systematic approach like the one illustrated in the following section with the *PPD*ˆ* results over whole summer seasons discussed in sections 5.3 and 5.4.

5.2. Changes in the dissatisfied percentage PPD over the whole season

We analyze here the full season evolution of the *PPD* through *PPD** in the sun, and *PPDˆ* in the shaded zones (see definitions 3.3). Considering diurnal hours over the 3-month period, we obtained 1288 georeferenced *UTCI* matrices, multiplied by the 6 tree planting strategies (Fig. 8). First,

we considered the dissatisfaction percentage in the sun and in the shade for the typical climate of La Rochelle and a tree canopy cover of 20%, given for all the days and the daytime hours by the following heat maps (Fig. 10).

These seasonal results (Fig. 10) are of interest to urban planners and decision makers who could identify when heat limits restricts the use of urban areas depending on the time of the day and the people vulnerability. In this case study, the critical hours typically occurred in mid-afternoon. The *PPD** (first heat map in Fig. 10) quickly reached values close to 100% under the sun, even early in the morning, while most of the season was quite comfortable in the shade (*PPDˆ*, second heat map in Fig. 10). There was always an minimum of about 5% dissatisfied people, which is consistent with the general *PPD* definition from Fig. 2.

We can clearly identify the warmest day, August 11, when the shaded areas were also uncomfortable for most pedestrians, which correlates with the highest air temperature, although there were very uncomfortable days at the beginning of August in the sunlit zones. It is not clear from the results which periods are critical, given that the very hot days of June or July might be almost completely bearable in terms of the *PPDˆ* in the shaded areas. Therefore, we suggest consolidating this information into a single representation through the use of the *PPD*ˆ* heatmap.

5.3. Results and analyses of the PPD*ˆ indicator

The overall dissatisfaction percentage (*PPD*ˆ*, defined in section 3.5) takes into account the relative availability of shaded areas, and the change from morning to evening, and during the season. For the same case study (20% tree coverage), the results of the *PPD*ˆ* can be compared with this general indicator during the summer season with the other tree coverage strategies, from 0% to 80% (Fig. 11).

As expected, the high percentage of dissatisfied people decreased with additional trees, especially from the 40% level. The no-tree scenario (0% tree cover) highlighted the critical days during the whole season, which could almost all be mitigated by this 40% ratio that was defined in section 3.4. However, even for the oceanic climate of La Rochelle, there were still 3 days, and especially one day, when the shading parameter and the increased tree cover were not high enough to completely mitigate the dissatisfaction percentage. A noticeable decrease in the *PPD*ˆ* is observed between August 11 and August 12, due to a significant drop in the air temperature ($T_{max} = 35.8°C$ on August 11 and 23.6°C on August 12).

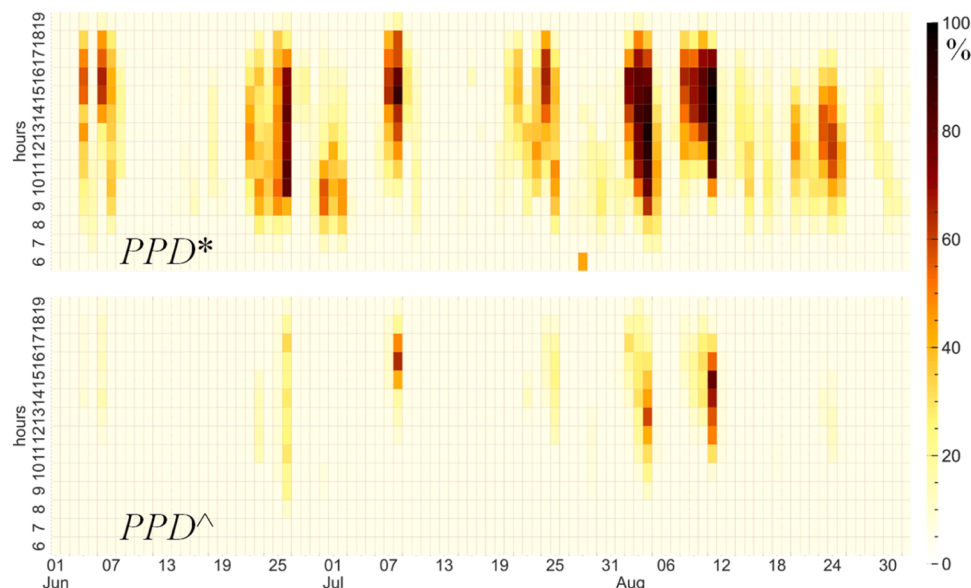**Fig. 10.** The dissatisfaction percentage indicators *PPD** and *PPDˆ* for the typical weather of La Rochelle, and a tree cover of 20%.

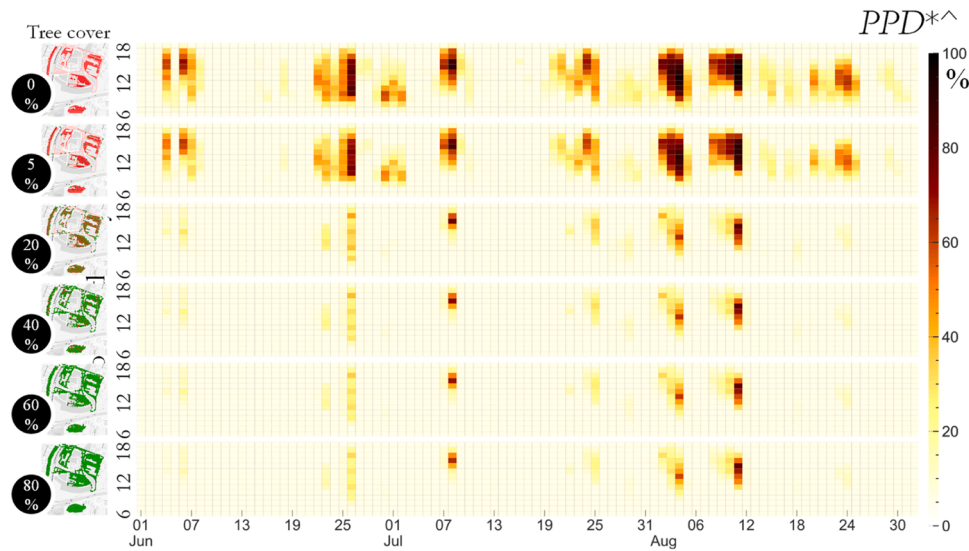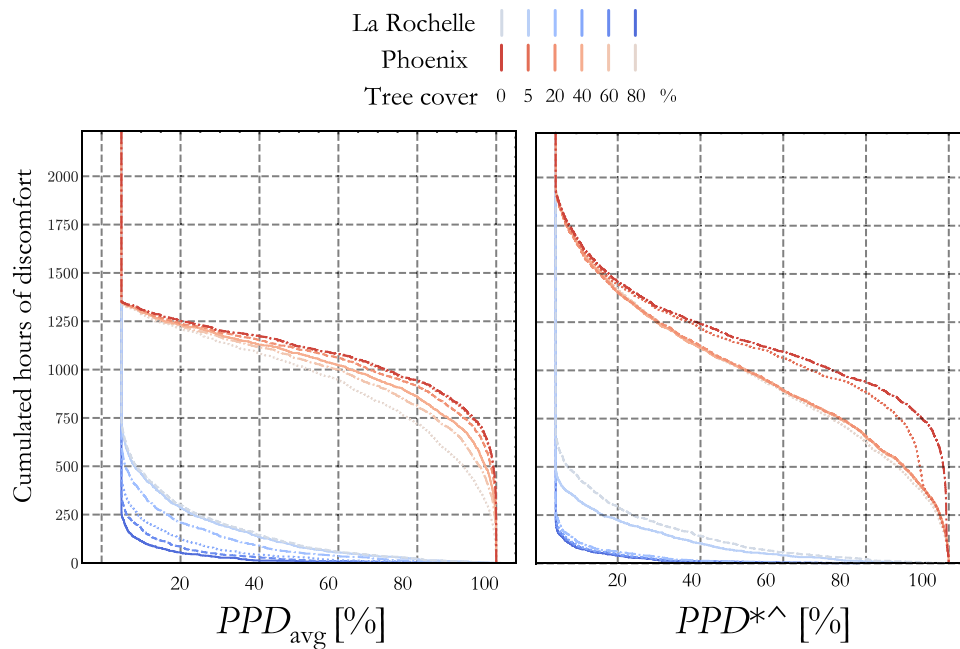**Fig. 11.** *PPD**^ for different tree covers, from 0 to 80%, for the typical weather of La Rochelle.

Fig. 12. Cumulative hours above a certain percentage of (a) the spatially averaged PPD_{avg} and (b) PPD*^ for both La Rochelle (blue) and Phoenix (red) climates.

The first result obtained with this methodology shows that the two extreme scenarios of the tree planting strategy (0 and 80%) gave an objective quantification of what is achievable in terms of daily and hourly cooling benefits, not only in terms of the difference between shaded and sunlit areas as previously analyzed with *PPD** and *PPD*^. This is not just the summer solstice, and although some days may be too hot, this must be put into perspective with what can be expected during the rest of the season when the open spaces can be used.

The second result is that the dissatisfied people percentage does not vary linearly with the tree cover ratio. Thus, even with an identical tree cover ratio $\hat{\sigma}_{forAll}$, the hottest hours and days will be different for two cities with two different climates, as will the threshold that can be identified through this representation of tree cover scenario (Fig. 11); this will be useful in deciding which scenario to apply.

5.4. Determining the cooling strategy performance in overheating hours

Another practical way to show the potential of the novel *PPD**^ indicator is to evaluate the number of hours below a threshold of global dissatisfaction that can be set by urban planners, who can then obtain an assessment of the overheating hours for any given assessed strategy. We took all the simulated tree planting strategies, from 0 to 80%, and the two climates of La Rochelle and Phoenix, and processed all the thermal discomfort and stress maps in the pedestrian areas to plot the cumulated hours below a given threshold of *PPD**^ (Fig. 12a), which we then compared with the same plot obtained with the averaged PPD_{avg} (Fig. 12b) in order to underline any difference in results. The PPD_{avg} is defined as the *PPD* calculated using the average *UTCI* in the neighborhood, where the *UTCI* is averaged between shaded and sunlit conditions, weighted by the respective surface areas.

The observed benefits of increased tree cover in terms of overheating

hours were less important with the simple averaged PPD_{avg} (Fig. 12a) than the results obtained with the $PPD*\hat{}$ (Fig. 12b), which more accurately accounted for the cooling benefits. Moreover, the gain in Fig. 12a is too simplistically proportional to the tree cover ratio, which is due to the fact that the averaged value PPD_{avg} does not take into account the combined effects of the increased number of people in shaded areas during hot events, which instead induced non-linear variations that are visible in Fig. 12b for the $PPD*\hat{}$ indicator. We can see in Fig. 12b that at low tree cover ratios (0% and 5%), the relative benefits were almost identical for both the La Rochelle and Phoenix climates, and that above 20% there was almost no increased benefit. While the benefits increased linearly with tree cover for PPD_{avg}. Thus, the simple averaged PPD_{avg} could lead to recommendations that overestimate the necessary amount of shading. Considering the 40% threshold for $PPD*\hat{}$ with 20% tree cover in Phoenix (red curve at 20% tree cover, Fig. 12b), we see that it is exceeded for about 1 100 hours (out of the 2 232 hours in the summer period, or 49% of the summer), while it was comfortable for almost the whole summer in La Rochelle (blue curve at 20% tree cover, Fig. 12b).

By incorporating theoretical occupancy patterns, the $PPD*\hat{}$ indicator provides a more nuanced and accurate representation of urban heat stress, which could lead to a reconsideration of the real benefits and limits of a given strategy such as the 20% tree canopy limit in this example. It would be particularly interesting to see how it might be possible to push the limits of shading strategies further by combining other urban cooling strategies, such as increased albedo or evaporative cooling. This type of analysis with the $PPD*\hat{}$ indicator would then be valuable in determining the optimal cost-benefit ratio for each strategy, and to guide urban planning and climate adaptation strategies more effectively.

6. Conclusions

Regarding the challenges identified in section 2, an important result of this paper is the proposed development and testing of a methodology to obtain a quantitative indicator $PPD*\hat{}$ that contributes to bridge the gaps between heat stress and the necessary shading ratio considering a global formula to assess the pedestrian dissatisfaction.

Regarding the first research question proposed in Section 2, we have set up a case study simulation of a specific neighborhood in order to demonstrate how the detailed thermal sensation maps can be analyzed in detail, even though it requires careful cross-analysis of the various thermophysical results (see Section 5.1). Like similar urban climate studies, we relied on perceived temperature maps, which bring detailed expertise when analyzed at each time step. This specifically highlights the complexity to have a systemic approach of the spatial and time variations of all climatic data. Mean radiant temperature plays a critical role for assessing outdoor thermal comfort. Shading strategies, integrated into urban policies, can significantly influence this parameter. The proposed $PPD*\hat{}$ indicator offers a step toward bridging the gap between detailed numerical analysis of thermal comfort through urban climate studies, and the much more practical urban planning approaches.

Regarding the second research question proposed in Section 2, we have developed in a first methodological approach this dissatisfaction percentage to aggregate the pedestrian usage pattern in a simplified way to evaluate the outdoor thermal comfort. It provides a preliminary estimate of the number of occupants likely to seek shade, based on the

assumption that shadings are available for everyone. These simplifications are important in order to develop a standardized approach, while uncertainties are high at the urban planning stage for new adaptation strategies. In the urban policy practice, our review (see Section 1.3) has highlighted a convergence of typical shading ratio targets. It is interesting to note that even these values were used as a reference for the parameterization of the model (see Section 3.4) the results highlighting that considering the thermal perception and the climate variability for a full summer season the optimal value could be different (see section 5.4). In further development steps, it would be interesting to further investigate this specific parameterization of the methodology and the $PPD*\hat{}$ results in comparison to the feelings and behavior of the pedestrians through detailed surveys. E.g., train station plazas or other typical places where while occupants are often required to wait outdoors under constrained conditions, with enough variety of pedestrians, are interesting perspectives for a relatively standardized approach and the development of a calibration procedure.

Regarding the perspectives on the thermal comfort modeling capabilities and the challenges opened by this proposed approach, we can consider future developments beyond the standardized and static thermal comfort approaches. Indeed, the $PPD*\hat{}$ could be further improved by considering more localized cooling effects with more than two clusters (sunlit and shaded), different types of activities (e.g., static versus moving pedestrians), more adequate assessment of the shaded area (e.g. taking into account the density of the neighborhood or the city which could initially be related to the building floor area), varying levels of occupancy during different times of the day and during the year. Moreover, the use of this integrated indicator could be further adapted to study the seasonal variations, potentially revealing distinct urbanization strategies thresholds compared to existing studies.

Finally, this article specifically focused on shading policies, though the proposed methodology can be applied to further study complimentary urban cooling strategies, such as misters or fountains that can greatly improve thermal comfort in shaded areas during overheating periods. Determining the optimal amount of shade for an urban project is not straightforward. Indeed, shade as a passive solution only provides cooling benefits within a certain temperature range. Beyond this range, high air temperatures can render outdoor spaces uncomfortable, even in shaded areas.

CRediT authorship contribution statement

Simon Martinez: Writing – original draft, Visualization, Software, Methodology, Investigation, Formal analysis, Conceptualization. **Marika Vellei:** Writing – review & editing, Writing – original draft, Methodology, Conceptualization. **Manon Rendu:** Writing – original draft, Resources, Project administration. **Boris Brangeon:** Software, Resources, Data curation. **Carlota Griffon:** Writing – original draft, Resources. **Emmanuel Bozonnet:** Writing – review & editing, Writing – original draft, Visualization, Supervision, Project administration, Methodology, Funding acquisition, Conceptualization.

Declaration of competing interest

The authors declare that they have no known competing financial interests or personal relationships that could have appeared to influence the work reported in this paper.
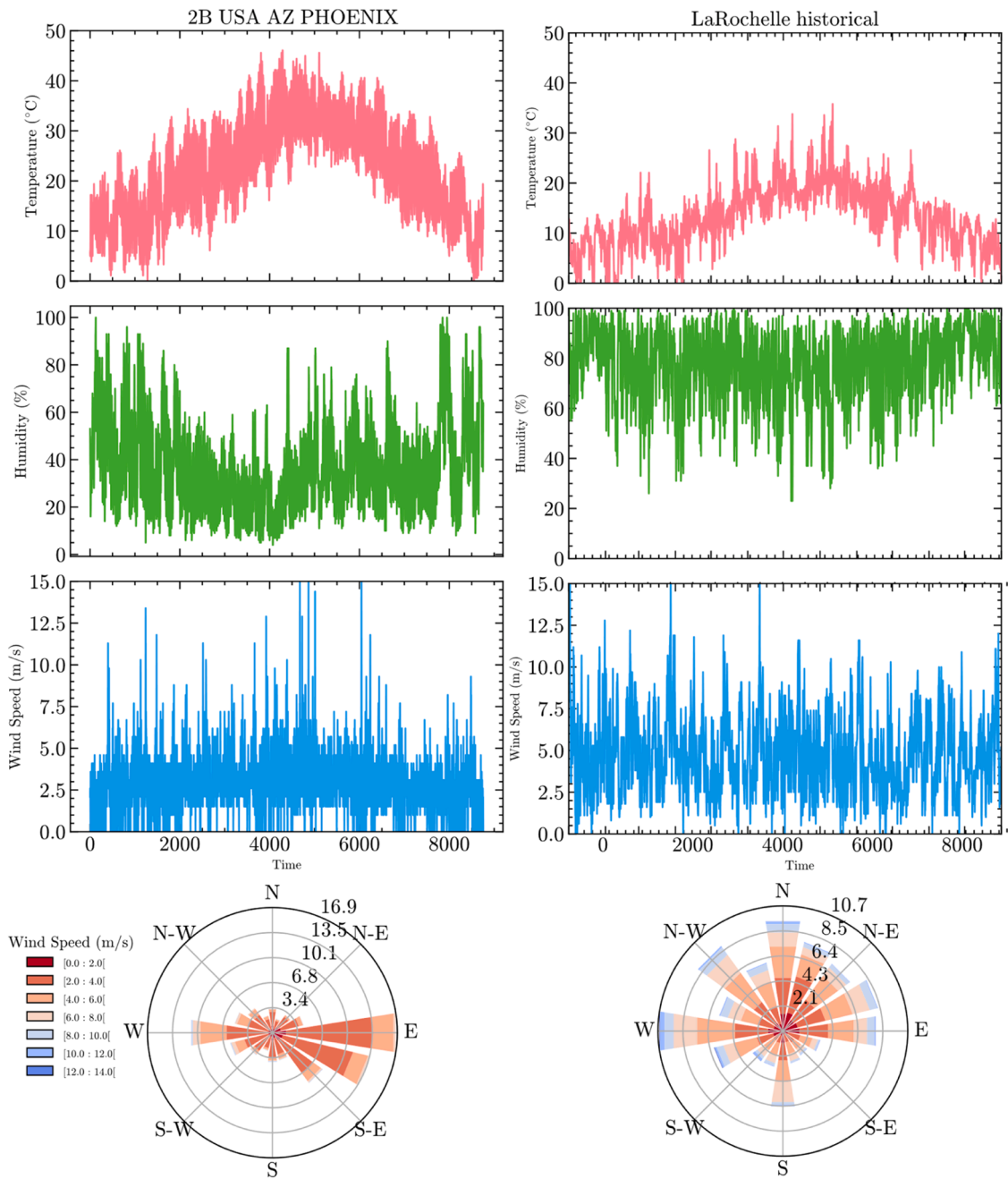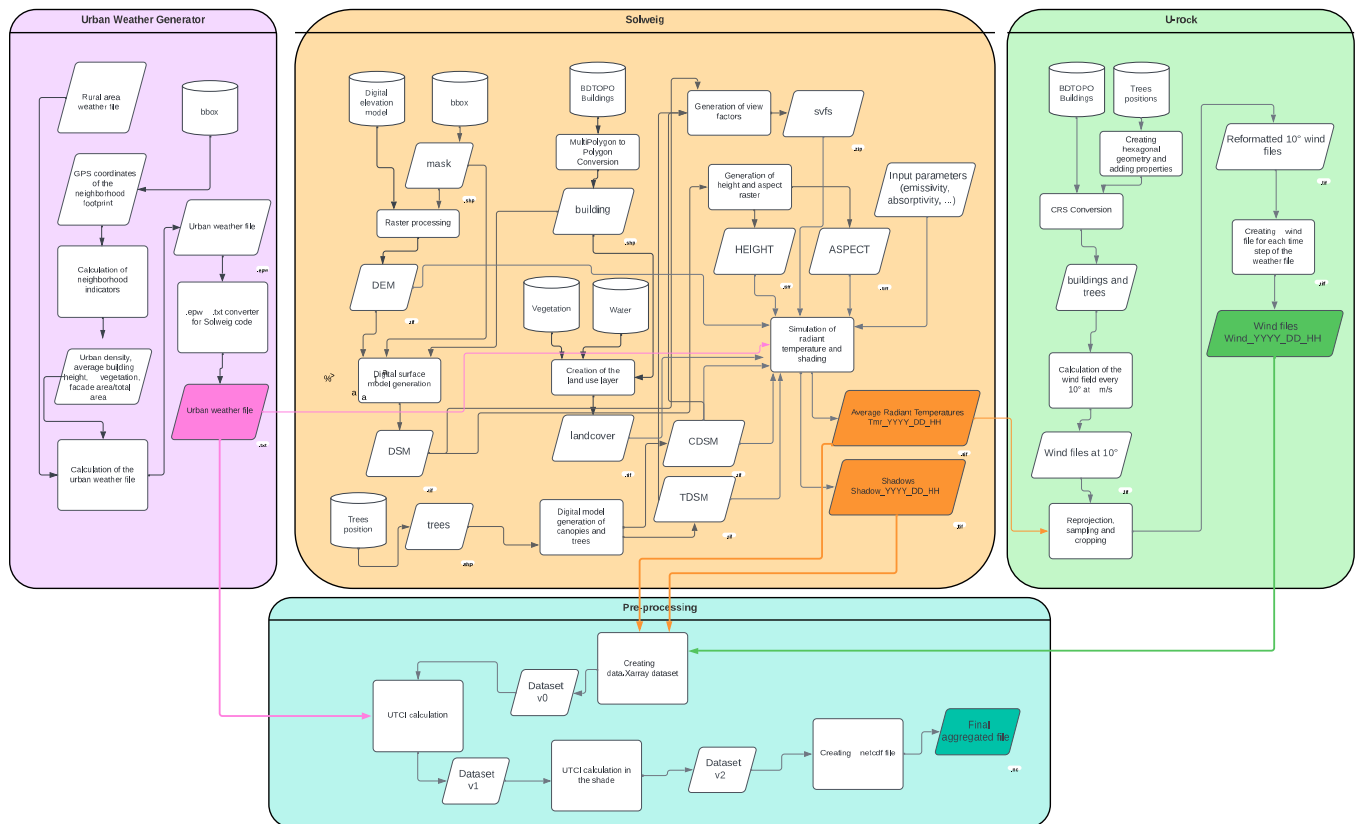
Appendix A

Fig. 13. Detailed weather data for both studied climates

Appendix B

This appendix details the inputs and outputs of the microclimate model described in section 3. The main parameters of each model are pre-processed from GIS data as described in the following diagram (Fig. 14), and the full numerical model is freely available (see github).

Fig. 14. Detailed diagram of model inputs and outputs for UWG, Solweig, and U-rock before the thermal comfort process (*UTCI*) - (https://github.com/rupeelab17/pymdu)

This diagram highlights the full process according to each software documentation, and the similarities and differences in the level of detail of the models for each purpose (urban air temperature for UWG, mean radiant temperature for Solweig, and urban wind field for U-Rock). The full definition of each parameter of the models is given in the following tables with the numerical values used in this study. Table 3 shows the neighborhood parameters for the urban temperature calculation with specific parameters for the UWG software as described in detail in the official documentation.

Table 3

main UWG inputs data (see doc https://urbanmicroclimate.scripts.mit.edu/uwg_parameters.php)

Description	UWG data	Value
Simulation start month (1-12)	month	1
Simulation start day (1-31)	day	1
Number of days to simulate	nday	365
Simulation timestep in seconds	dtsim	300
Meteorological data timestep in seconds	dtweather	3600
Sensible heat generated per occupant (W)	sensocc	100
Fraction of latent heat generated per occupant	latfocc	0.3
Fraction of radiant heat generated per occupant	radfocc	0.2
Fraction of radiant heat generated by equipment	radfequip	0.5
Fraction of radiant heat generated by electric lighting	radflight	0.7
Daytime urban boundary layer height (m)	h_ubl1	1000
Nighttime urban boundary layer height (m)	h_ubl2	80
Inversion height (m)	h_ref	150
Temperature measurement height (m)	h_temp	2
Wind measurement height (m)	h_wind	10
Wind scaling coefficient	c_circ	1.2
Exchange velocity coefficient	c_exch	1
Maximum daytime heat flux threshold (W/m²)	maxday	150
Maximum nighttime heat flux threshold (W/m²)	maxnight	20
Minimum wind speed (m/s)	windmin	1
Average height of rural obstacles (m)	h_obs	0.1
Height of urban buildings (m)	bldheight	7.3316
Fraction of HVAC heat lost to the street	h_mix	1
Building occupancy density	blddensity	0.14465
Urban area vertical/horizontal ratio	vertohor	0.26879
Urban characteristic length (m)	charlength	1000
Urban road albedo	albroad	0.1
Urban pavement thickness (m)	droad	0.5
Sensible anthropogenic heat at street level (W/m²)	sensanth	20

(continued on next page)

Table 3 (*continued*)

Description	UWG data	Value
Fraction of urban ground covered by grass	grasscover	0.07062
Fraction of urban ground covered by trees	treecover	0.1
Evapotranspiration start month	vegstart	4
Evapotranspiration end month	vegend	10
Vegetation albedo	albveg	0.25
Fraction of rural vegetation cover	rurvegcover	0.9
Fraction of latent heat absorbed by urban grass	latgrss	0.44
Fraction of latent heat absorbed by urban trees	lattree	0.6
Anthropogenic thermal load schedule - week days – Saturday – Sunday	schtraffic	((0.2. 0.2. 0.2. 0.2. 0.2. 0.4. 0.7. 0.9. 0.9. 0.6. 0.6. 0.6. 0.6. 0.6. 0.7. 0.8. 0.9. 0.9. 0.8. 0.8. 0.7. 0.3. 0.2. 0.2), (0.2. 0.2. 0.2. 0.2. 0.2. 0.3. 0.5. 0.5. 0.5. 0.5. 0.5. 0.5. 0.5. 0.5. 0.6. 0.7. 0.7. 0.7. 0.7. 0.5. 0.4. 0.3. 0.2. 0.2), (0.2. 0.2. 0.2. 0.2. 0.2. 0.3. 0.4. 0.4. 0.4. 0.4. 0.4. 0.4. 0.4. 0.4. 0.4. 0.4. 0.4. 0.4. 0.4. 0.4. 0.4. 0.3. 0.3. 0.2. 0.2))
Pavement thermal conductivity (W/m-K)	kroad	1
Pavement volumetric heat capacity (J/m³K)	croad	1600000
Matrix representing the fraction of urban building stock	bld	(('largeoffice', 'pst80', 0.4), ('midriseapartment', 'pst80', 0.6))

Table 4 is specific to the wind modeling data, the same neighborhood is represented with its morphology only as detailed in the UROCK documentation. I.e., some elements like buildings or trees are represented in both models but not with the same parameters, because the UWG model considers integrated morphological parameters, while the wind model of U-Rock considers the simplified 3D shapes, e.g. cylinders for trees.
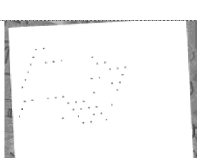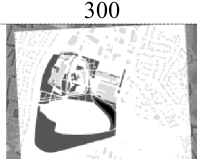
Table 4
main U-Rock input data (see documentation https://umep-docs.readthedocs.io/en/latest/processor/Wind%20model%20URock.html)

U-Rock data	Value	Description
BUILDINGS		Building – *shape file*
VEGETATION		Vegetation – *shape file*
VEGETATION_CROWN_TOP_HEIGHT	5.8	Field indicating maximum height of vegetation crown
VEGETATION_CROWN_BASE_HEIGHT	2.2	Field indicating minimum height of vegetation crown
ATTENUATION_FIELD	2.8	Field for attenuation factor
INPUT_WIND_HEIGHT	10	Wind input height (m)
INPUT_WIND_SPEED	1	Wind input speed (m/s)
INPUT_WIND_DIRECTION	0	Wind input direction (degrees)
HORIZONTAL_RESOLUTION	2	Horizontal resolution (m)
VERTICAL_RESOLUTION	2	Vertical resolution (m)
WIND_HEIGHT	1.5	Wind calculation height (m)

Following the Solweig pre-process to prepare the radiative input data, Table 5 gives an overview of the inputs that were used in this study for this model. Here, most of the numerical inputs are given by *geoTIFF* file formats that are processed from the publicly available GIS database, e.g. BDtopo (see the general procedure described in Section 3), for the case study specific location.

Table 5
main SOLWEIG input data (see also https://umep-docs.readthedocs.io/en/latest/OtherManuals/SOLWEIG.html)

SOLWEIG data	Value	Description
INPUT_DSM		Digital surface model (DSM) *geoTIFF file*
INPUT_SVF		sky view factors (SVF) *Zip file* containing *geoTIFF files*
INPUT_HEIGHT		Digital height model (HEIGHT) *geoTIFF file*
INPUT_ASPECT		Digital orientation model (ASPECT) *geoTIFF file*
INPUT_CDSM INPUT_TDSM		Digital surface model with vegetation (CDSM) Thermal digital surface model (TDSM) *geoTIFF files*
TRANS_VEG	3	Vegetation transmission (%)
LEAF_START	97	Start day of the foliar period
LEAF_END	300	End day of the foliar period
INPUT_LC		Land cover *geoTIFF file*
INPUT_DEM		Digital elevation model (DEM) *geoTIFF file*
ALBEDO_WALLS	0.2	Wall albedo
ALBEDO_GROUND	0.15	Soil albedo
EMIS_WALLS	0.9	Wall emissivity
EMIS_GROUND	0.95	Soil emissivity
ABS_S	0.7	Solar absorption
ABS_L	0.95	Longwave absorption

Data availability

Data will be made available on request.

References

Akbari, H., Pomerantz, M., & Taha, H. (2001). Cool surfaces and shade trees to reduce energy use and improve air quality in urban areas. *Solar Energy, 70*, 295–310. https://doi.org/10.1016/S0038-092X(00)00089-X

Aleksandrowicz, O., & Pearlmutter, D. (2023). The significance of shade provision in reducing street-level summer heat stress in a hot Mediterranean climate. *Landscape and Urban Planning, 229*, Article 104588. https://doi.org/10.1016/j.landurbplan.2022.104588

Aleksandrowicz, O., Zur, S., Lebendiger, Y., & Lerman, Y. (2020). Shade maps for prioritizing municipal microclimatic action in hot climates: Learning from Tel Aviv-Yafo. *Sustainable Cities and Society, 53*, Article 101931. https://doi.org/10.1016/j.scs.2019.101931

2017 ASHRAE Handbook: Fundamentals, American Society of Heating, Refrigerating and Air-Conditioning Engineers, 2017.

Barone, F., Merlier, L., Bouquerel, M., Kuznik, F. Heat Stress Assessment Using an Urban Microclimate Zonal Model at the Block Scale Coupled with Building Models, (2024). https://papers.ssrn.com/abstract=4921298 (accessed August 20, 2024).

Basu, R. (2009). High ambient temperature and mortality: a review of epidemiologic studies from 2001 to 2008. *Environmental Health, 8*, 40. https://doi.org/10.1186/1476-069X-8-40

Bernard, J., Lindberg, F., & Oswald, S. (2023). URock 2023a: an open-source GIS-based wind model for complex urban settings. *Geoscientific Model Development, 16*, 5703–5727. https://doi.org/10.5194/gmd-16-5703-2023

Bertrand, P., Debizet, G., Pezet-Kuhn, M., Daste, A., Henry, E., Chesne, L., Boite à Outils Air Climat Urbanisme, (2014). https://shs.hal.science/halshs-01875100 (accessed February 28, 2024).

Bestimmung der Strömungsverhältnisse im Bereich komplexer Bebauungsstrukturen, 1990.

Bozonnet, E., Musy, M., Calmet, I., & Rodriguez, F. (2015). Modeling methods to assess urban fluxes and heat island mitigation measures from street to city scale. *International Journal of Low-Carbon Technologies, 10*, 62–77. https://doi.org/10.1093/IJLCT/CTT049

Bröde, P., Fiala, D., Błażejczyk, K., Holmér, I., Jendritzky, G., Kampmann, B., Tinz, B., & Havenith, G. (2012). Deriving the operational procedure for the Universal Thermal Climate Index (UTCI). *Int J Biometeorol, 56*, 481–494. https://doi.org/10.1007/s00484-011-0454-1

Bueno, B., Norford, L., Hidalgo, J., & Pigeon, G. (2012). The urban weather generator. *Journal of Building Performance Simulation, 6*, 269–281, 10/gfkd9d.

Bueno, B., Norford, L., Hidalgo, J., & Pigeon, G. (2013). The urban weather generator. *Journal of Building Performance Simulation, 6*, 269–281. https://doi.org/10.1080/19401493.2012.718797

Buo, I., Sagris, V., Jaagus, J., & Middel, A. (2023). High-resolution thermal exposure and shade maps for cool corridor planning. *Sustainable Cities and Society, 93*, Article 104499. https://doi.org/10.1016/j.scs.2023.104499

City of Phoenix, City of Phoenix Tree and Shade Master Plan, City of Phoenix, USA, 2010. https://www.phoenix.gov/parkssite/Documents/PKS_Forestry/PKS_Forestry_Tree_and_Shade_Master_Plan.pdf (accessed August 20, 2024).

City of Phoenix, Street Transportation Cool Corridors Program, 2022. https://www.phoenix.gov:443/streets/coolcorridors (accessed August 20, 2024).

City of Phoenix, Chapter 13 Walkable Urban Code | Phoenix Zoning Ordinance, 2024. https://phoenix.municipal.codes/ZO/1304 (accessed August 20, 2024).

Coccolo, S., Kämpf, J., Scartezzini, J.-L., & Pearlmutter, D. (2016). Outdoor human comfort and thermal stress: A comprehensive review on models and standards. *Urban Climate, 18*, 33–57, 10/gdb9c3.

Dhalluin, A., & Bozonnet, E. (2015). Urban heat islands and sensitive building design – a study in some French cities' context. *Sustainable Cities and Society, 19*, 292–299. https://doi.org/10.1016/J.SCS.2015.06.009

Ding, X., Zhao, Y., Strebel, D., Fan, Y., Ge, J., & Carmeliet, J. (2024). A WRF-UCM-SOLWEIG framework for mapping thermal comfort and quantifying urban climate drivers: Advancing spatial and temporal resolutions at city scale. *Sustainable Cities and Society, 112*, Article 105628. https://doi.org/10.1016/j.scs.2024.105628

Fard, B. Jalalzadeh, Mahmood, R., Hayes, M., Rowe, C., Abadi, A. M., Shulski, M., Medcalf, S., Lookadoo, R., & Bell, J. E. (2021). Mapping Heat Vulnerability Index Based on Different Urbanization Levels in Nebraska, USA. *GeoHealth, 5*, Article e2021GH000478. https://doi.org/10.1029/2021GH000478

Government of Dubai, Dubai Building Code (DBC), 2021. https://www.dm.gov.ae/municipality-business/planning-and-construction/dubai-building-code-2/(accessed August 21, 2024).

Havenith, G., Fiala, D., Błażejczyk, K., Richards, M., Bröde, P., Holmér, I., Rintamaki, H., Benshabat, Y., & Jendritzky, G. (2012). The UTCI-clothing model. *Int J Biometeorol, 56*, 461–470. https://doi.org/10.1007/s00484-011-0451-4

Huang, J., Chen, Y., Jones, P., & Hao, T. (2022). Heat stress and outdoor activities in open spaces of public housing estates in Hong Kong: A perspective of the elderly community. *Indoor and Built Environment, 31*, 1447–1463. https://doi.org/10.1177/1420326X20950448

Hwang, R.-L., Weng, Y.-T., & Huang, K.-T. (2022). Considering transient UTCI and thermal discomfort footprint simultaneously to develop dynamic thermal comfort models for pedestrians in a hot-and-humid climate. *Building and Environment, 222*, Article 109410. https://doi.org/10.1016/j.buildenv.2022.109410

Inostroza, L., Palme, M., & de la Barrera, F. (2016). A Heat Vulnerability Index: Spatial Patterns of Exposure, Sensitivity and Adaptive Capacity for Santiago de Chile. *PLOS ONE, 11*, Article e0162464. https://doi.org/10.1371/journal.pone.0162464

Katić, K., Li, R., & Zeiler, W. (2016). Thermophysiological models and their applications: A review. *Building and Environment, 106*, 286–300. https://doi.org/10.1016/j.buildenv.2016.06.031

Konarska, J., Lindberg, F., Larsson, A., Thorsson, S., & Holmer, B. (2014). Transmissivity of solar radiation through crowns of single urban trees—application for outdoor thermal comfort modelling. *Theor Appl Climatol, 117*, 363–376. https://doi.org/10.1007/s00704-013-1000-3

Li, Y., Lin, D., Zhang, Y., Song, Z., Sha, X., Zhou, S., Chen, C., & Yu, Z. (2023). Quantifying tree canopy coverage threshold of typical residential quarters considering human thermal comfort and heat dynamics under extreme heat. *Building and Environment, 233*, Article 110100. https://doi.org/10.1016/j.buildenv.2023.110100

Lindberg, F., Holmer, B., & Thorsson, S. (2008). SOLWEIG 1.0 – Modelling spatial variations of 3D radiant fluxes and mean radiant temperature in complex urban settings. *Int J Biometeorol, 52*, 697–713. https://doi.org/10.1007/s00484-008-0162-7

Martinez, S., Machard, A., Pellegrino, A., Touili, K., Servant, L., & Bozonnet, E. (2021). A practical approach to the evaluation of local urban overheating– A coastal city case-study. *Energy and Buildings, 253*, Article 111522. https://doi.org/10.1016/j.enbuild.2021.111522

Middel, A., Lukasczyk, J., & Maciejewski, R. (2017). Sky View Factors from Synthetic Fisheye Photos for Thermal Comfort Routing—A Case Study in Phoenix, Arizona. *Urban Planning, 2*, 19–30. https://doi.org/10.17645/up.v2i1.855

Migliari, M., Babut, R., De Gaulmyn, C., Chesne, L., & Baverel, O. (2022). The Metamatrix of Thermal Comfort: A compendious graphical methodology for appropriate selection of outdoor thermal comfort indices and thermo-physiological models for human-biometeorology research and urban planning. *Sustainable Cities and Society, 81*, Article 103852. https://doi.org/10.1016/j.scs.2022.103852

Nakano, A., Bueno, B., Norford, L., & Reinhart, C. F. (2015). *Urban Weather Generator - a Novel Workflow for Integrating Urban Heat Island Effect within Urban Design Process*. MIT Web Domain. https://dspace.mit.edu/handle/1721.1/108779 accessed February 22, 2024.

NetZeroCities, Home, Towards Climate Neutral European Cities by 2030 (n.d.). https://netzerocities.eu/(accessed August 20, 2024).

Peeters, A., Shashua-Bar, L., Meir, S., Shmulevich, R. R., Caspi, Y., Weyl, M., Motzafi-Haller, W., & Angel, N. (2020). A decision support tool for calculating effective shading in urban streets. *Urban Climate, 34*, Article 100672. https://doi.org/10.1016/j.uclim.2020.100672

Psikuta, A., Fiala, D., Laschewski, G., Jendritzky, G., Richards, M., Błażejczyk, K., Mekjavič, I., Rintamäki, H., de Dear, R., & Havenith, G. (2012). Validation of the Fiala multi-node thermophysiological model for UTCI application. *Int J Biometeorol, 56*, 443–460. https://doi.org/10.1007/s00484-011-0450-5

Rüdisser, D., Weiss, T., & Unger, L. (2021). Spatially Resolved Analysis of Urban Thermal Environments Based on a Three-Dimensional Sampling Algorithm and UAV-Based Radiometric Measurements. *Sensors, 21*, 4847. https://doi.org/10.3390/s21144847

Rockle, R. (1990). *Bestimmung der Stomungsverhaltnisse im Bereich komplexer Bebauungsstrukturen*. Germany: Vom Fachbereich Mechanik, der Technischen Hochschule Darmstadt. Ph.D. thesis.

Romero Lankao, P., & Qin, H. (2011). Conceptualizing urban vulnerability to global climate and environmental change. *Current Opinion in Environmental Sustainability, 3*, 142–149. https://doi.org/10.1016/j.cosust.2010.12.016

Sampson, N. R., Gronlund, C. J., Buxton, M. A., Catalano, L., White-Newsome, J. L., Conlon, K. C., O'Neill, M. S., McCormick, S., & Parker, E. A. (2013). Staying cool in a changing climate: Reaching vulnerable populations during heat events. *Glob Environ Change, 23*, 475–484. https://doi.org/10.1016/j.gloenvcha.2012.12.011

Santamouris, M. (2020). Recent progress on urban overheating and heat island research. Integrated assessment of the energy, environmental, vulnerability and health impact. Synergies with the global climate change. *Energy and Buildings, 207*, Article 109482. https://doi.org/10.1016/j.enbuild.2019.109482

Singh, B., Hansen, B., Brown, M., & Pardyjak, E. (2008). Evaluation of the QUIC-URB fast response urban wind model for a cubical building array and wide building street canyon. *Environmental Fluid Mechanics, 8*, 281–312. https://doi.org/10.1007/s10652-008-9084-5

Singh, R., Arrighi, J., Jjemba, E., Strachan, K., Spires, M., & Kadihasanoglu, A. (2019). *Heatwave guide for cities*. Red Cross Red Crescent Climate Centre.

Tartarini, F., & Schiavon, S. (2020). pythermalcomfort: A Python package for thermal comfort research. *SoftwareX, 12*, Article 100578. https://doi.org/10.1016/j.softx.2020.100578

Turner, V. K., Middel, A., & Vanos, J. K. (2023). Shade is an essential solution for hotter cities. *Nature, 619*, 694–697. https://doi.org/10.1038/d41586-023-02311-3

Ulpiani, G., Treville, A., Bertoldi, P., Vetters, N., Barbosa, P., Feyen, L., Naumann, G., & Santamouris, M. (2024). Are cities taking action against urban overheating? Insights from over 7,500 local climate actions. *One Earth, 7*, 848–866. https://doi.org/10.1016/j.oneear.2024.04.010

United Nations, Department of Economic and Social Affairs, Population Division (2022), 2022 Revision of World Population Prospects, (n.d.). https://population.un.org/wpp/.

Urban Forest Strategy 2014, (n.d.).

Urban Redevelopment Authority (Singapore), Gross Floor Area Handbook (GFA), 2023. https://www.ura.gov.sg/Corporate/Guidelines/Development-Control/gross-floor-area/GFA/Privately-OwnedPublicSpacesPOPS (accessed August 21, 2024).

Vandentorren, S., Suzan, F., Medina, S., Pascal, M., Maulpoix, A., Cohen, J.-C., & Ledrans, M. (2004). Mortality in 13 French Cities During the August 2003 Heat Wave. *American Journal of Public Health, 94*, 1518–1520. https://doi.org/10.2105/AJPH.94.9.1518

Wilhelmi, O. V., & Hayden, M. H. (2010). Connecting people and place: a new framework for reducing urban vulnerability to extreme heat. *Environ. Res. Lett., 5*, Article 014021. https://doi.org/10.1088/1748-9326/5/1/014021